6624 *Chem. Mater.* **2010,** *22,* 6624–6631
DOI:10.1021/cm1020977

CHEMISTRY OF MATERIALS
Article

Niobium Doped TiO_2 with Mesoporosity and Its Application for Lithium Insertion

Yude Wang,*[,†] Bernd M. Smarsly,[‡] and Igor Djerdj[§]

[†]*Department of Materials Science and Engineering, Yunnan University, 650091 Kunming, People's Republic of China,* [‡]*Institute of Physical Chemistry, Justus-Liebig-University Giessen, Heinrich-Buff-Ring 58, D-35392 Giessen, Germany, and* [§]*Division of Materials Physics, Ruđer Bošković Institute, Bijenička 54, 10000 Zagreb, Croatia*

Received July 28, 2010. Revised Manuscript Received November 8, 2010

The synthesis as well as the electrochemical properties study of niobium-doped TiO_2 (NTO) with mesoporosity and high surface area is presented. The mesoporous NTO was prepared using a novel poly(ethylene-*co*-butylene)-*b*-poly(ethylene oxide) amphiphilic diblock copolymer as a template and simple titanium reagents ($TiCl_4$ and $Nb(OC_2H_5)_5$) by a polymer-assisted sol−gel process. The samples were characterized by differential scanning calorimetry and thermogravimetric analysis (DSC-TGA), X-ray diffraction (XRD), Fourier transformed infrared (FTIR) spectroscopy, scanning electron microscopy (SEM), transmission electron microscopy (including high-resolution imaging-HRTEM), and the Brunauer−Emmett−Teller (BET). All samples are highly crystalline and have pore-solid architectures after removal of the polymer template by calcination. The resulting mesoporous NTO shows a high porosity of 46% and a high surface area of 128 m^2/g, respectively. The as-prepared samples were used as positive electrode materials for lithium-ion battery, whose charge−discharge properties, cyclic voltammetry, and cycle performance were examined and revealed very good properties. A highly stable capacity of 160 mA h g^{-1} was found after 100 cycles.

Introduction

Titanium dioxide (TiO_2) as an important, wide band gap semiconductor has been intensively studied as a key material for fundamental research and technological applications in the fields of semiconductors, optical devices,[1] photovoltaic cells,[2] photocatalysis,[3] gas sensing,[4] and electrochemical storage.[5] TiO_2 is a typical Li-ion intercalation compound with a volume change $<4\%$ in the reaction described by eq 1:

$$TiO_2 + xLi^+ + xe^- \leftrightarrow Li_xTiO_2 \quad (0 \le x \le 1) \qquad (1)$$

Particularly, nanostructured TiO_2 for Li insertion has received much attention because of its low-voltage insertion host for Li and the fast Li insertion/extraction host.[6] These characteristics make it a potential anode material for high-power lithium-ion batteries, avoiding the necessity of a passivation layer at the contact to the liquid electrolyte.[7] However, TiO_2 has low electric conductivity that limits its use for high power output.

A number of studies have been performed on electrical properties of TiO_2, and it is well-known that electrical conductivity is sensitive to the presence of aliovalent ions.[8] This effect has been recently studied in detail for both donor-type addition (Nb)[9] and acceptor-type additions (Cr).[10] It has been generally assumed that the effect of aliovalent ions on the electrical conductivity is mainly related to their effect on the concentration of electronic charge carriers, while the effect on the mobility terms is insignificant.[8,11] The substitutional doping of TiO_2 with niobium ions has a profound effect on electrical conductivity

*To whom correspondence should be addressed. E-mail: ydwang@ynu.edu.cn.

(1) Naoi, K.; Ohko, Y.; Tatsuma, T. *J. Am. Chem. Soc.* **2004**, *126*, 3664.
(2) (a) O'Regan, B.; Grätzel, M. *Nature* **1991**, *353*, 737. (b) Adachi, M.; Murata, Y.; Takao, J.; Jiu, J.; Sakamoto, M.; Wang, F. *J. Am. Chem. Soc.* **2004**, *126*, 14943. (c) Mor, G. K.; Shankar, K.; Paulose, M.; Varghese, O. K.; Grimes, C. A. *Nano Lett.* **2006**, *6*, 215.
(3) (a) Cao, Y.; Zhang, X.; Yang, W.; Du, H.; Bai, Y.; Li, T.; Yao, J. *Chem. Mater.* **2000**, *12*, 3445. (b) Sakthivel, S.; Kisch, H. *Angew. Chem., Int. Ed.* **2003**, *42*, 4908.
(4) (a) Wu, N.; Wang, S.; Rusakova, I. *Science* **1999**, *285*, 1375. (b) Du, X.; Wang, Y.; Mu, Y.; Gui, L.; Wang, P.; Tang, Y. *Chem. Mater.* **2002**, *14*, 3953.
(5) (a) Fujishima, A.; Honda, K. *Nature* **1972**, *238*, 37. (b) Boschloo, G. K.; Goossens, A.; Schoonman, J. *J. Electrochem. Soc.* **1997**, *144*, 1311.
(6) Hu, Y. S.; Kienle, L.; Guo, Y. G.; Maier, J. *Adv. Mater.* **2006**, *18*, 1421.
(7) (a) Kavan, L.; Grätzel, M.; Gilbert, S. E.; Klemenz, C.; Scheel, H. J. *J. Am. Chem. Soc.* **1996**, *118*, 6716. (b) Wagemaker, M.; van de Krol, R.; Kent-gens, A. P. M.; Well, A. A.; Mulder, F. M. *J. Am. Chem. Soc.* **2001**, *123*, 11454. (c) Wagemaker, M.; Kentgens, A. P. M.; Mulder, F. M. *Nature* **2002**, *418*, 397. (d) Armstrong, A. R.; Armstrong, G.; Canales, J.; Garcia, R.; Bruce, P. G. *Adv. Mater.* **2005**, *17*, 862.
(8) Kofstad, P. *Nonstoichiometry, Diffusion and Electrical Conductivity of Binary Metal Oxides*; Wiley-Interscience: New York, 1972; pp 81−109.
(9) Sheppard, L. R.; Bak, T.; Nowotny, J. *J. Phys. Chem. B* **2006**, *110*, 22447.
(10) Carpentier, J. L.; Lebrun, A.; Perdu, F. *J. Phys. Chem. Solids* **1989**, *50*, 145.
(11) Bak, T.; Nowotny, M. K.; Sheppard, L. R.; Nowotny, J. *J. Phys. Chem. C* **2008**, *112*, 7255.

 Published on Web 11/24/2010

and will drastically increase electrical conductivity of the titania.[12] Recent technological interest in Nb-doped TiO_2 derives from the fact that Nb doping leads to enhanced photocatalytic activity in the destruction of organochloride pollutants,[13] enhanced catalytic activity in the reduction of NO by NH_3,[14] and improved response in the sensing of O_2 and H_2.[15] On the other hand, research interests in developing mesoporous TiO_2 to further improve the electrochemical performance are arising, and fabrication of mesoporous titania and application in lithium-ion batteries have been reported.[16] Compared with conventional nanoparticulate system, the new anode material has not only a high surface area, a smooth neck structure of nanocrystals along the framework, but also uniform continuous nanochannels. The mesoporous TiO_2 showed very desirable electrochemical performance, which was attributed to the regular porosity which enabled thorough flooding of the electrolyte and voidage in the mesopores for buffering volume expansion. The open, mesoporous structure, efficient transport of lithium ions and effective ion-exchange properties result in a high value of charge/discharge capacity and fast kinetics together with high robustness and good safety characteristics.[17] However, to our knowledge, the electrochemical behavior of mesostructured Nb-doped TiO_2 used as a potential anode material for lithium-ion batteries has not been reported.

Polymer and surfactant templating provides a unique, simple method for producing ordered porous inorganic materials with precisely defined nanoscale architectures. Such materials can be readily formed as either bulk powders or thin films by solution phase coassembly of inorganic oligomers with amphiphilic surfactants or block copolymers.[18] In the present paper, we first synthesized and characterized the mesoporous Nb-doped TiO_2 with various Nb contents (0, 2.5, 5.0, 6.5, 10, 15, and 20 at %) and thermally treated at 470 °C. Then, we report the electrochemical behavior (charge−discharge properties, cyclic voltammetry, and cycle performance) as positive electrode materials for a lithium-ion battery. On the basis of our preliminary experiments, the mesoporous Nb-doped TiO_2 with 6.5 at % Nb content was found to be the most promising for the electrochemical behavior (Table S1 of the Supporting Information). In this paper, we mainly discuss the NTO sample doped with 6.5% Nb content.

Experimental Section

Materials. $TiCl_4$ (99.9%) and $Nb(OC_2H_5)_5$ (99.95%) were purchased from Sigma-Aldrich. $H(CH_2CH_2CH_2(CH)CH_2CH_3)_{89}(OCH_2CH_2)_{79}OH$ (referred to as KLE22)[19] was used as organic templates. All the chemical reagents used in the experiments were obtained from commercial sources as guaranteed-grade reagents and used without further purification.

Synthesis. NTO powders with a 6.5% molar ratio Nb were prepared because the ratio was found to be the most promising for the electrochemical performance in our incipient experiments. In a water-free container, the initial solutions were prepared by dissolving 600 mg of $TiCl_4$ and 6.3% molar ratio $Nb(OC_2H_5)_5$ in 4 mL of EtOH. The isotropic solutions containing 37.2 wt % of the amphiphilic block-copolymer KLE22, with respect to the amount of titanium oxide formed, were dissolved in the proper amount of EtOH−THF. The resulting sol mixed inorganic precursors and polymer template was stirred for 4 h and aged for 48 h before it was used to prepare the powders. The sol was poured into a Petri dish with a diameter of 9 cm and dried in air at room temperature for 24 h so that the most of the solvent was gone via evaporation. The resulting material was heated at 150 °C for 24 h. Afterward, the remaining substrates were scratched from the Petri dish. The product was heated at 300 °C with a ramp of 1 °C/min for 2 h. Finally, the dried piece of the mixed material was calcined at 470 °C for 2 h with a ramp of 2 °C/min to remove all the organics. The oven was cooled down to room temperature automatically without any additional cooling system.

Methods. Powder X-ray diffraction (XRD) data were carried out with a D8 diffractometer from Bruker instruments (Cu−Kα radiation) in reflection mode. The sample was scanned from 20° to 65° (2θ) in steps of 0.05°. The crystallite domain sizes (D) have been examined from XRD peaks based on Scherrer's equation: $D = 0.9\lambda/(\Delta W \cos\theta)$, where λ is the wavelength of X-ray ($\lambda = 0.154\,18$ nm), θ is the Bragg's diffraction angle, and ΔW is the true half-peak width of the X-ray diffraction lines. The recorded XRD powder patterns were processed with the Rietveld method using the program FULLPROF. The details were performed as previously reported.[20] The differential scanning calorimetry and thermogravimetric analysis (DSC-TGA) curves were obtained in flowing air on NETZSCH STA 409 PG/PC with a temperature increase rate of 10 °C/min. X-ray photoelectron spectroscopy (XPS) was measured at room temperature in ESCALAB 250. During XPS analysis, the Al Kα X-ray beam was adopted as the excitation source and power was set to 250 W. Vacuum pressure of the instrument chamber was 1×10^{-7} Pa as read on the panel. Measured spectra were decomposed into Gaussian components by a least-squares fitting method. Bonding energy was calibrated with reference to the C1s peak (285.0 eV). The transmission electron microscopy (TEM) has been performed on a Zeiss EM 912Ω instrument at an acceleration voltage of 120 kV, while a high-resolution transmission electron microscopy (HRTEM) characterization was done using a Philips CM200-FEG microscope (200 kV, $C_s = 1.35$ mm). The samples for TEM were prepared by dispersing the final powders in ethanol; this dispersing was then dropped on carbon−copper grids. Scanning electron microscopy (SEM) images of the morphology of particles were obtained from A LEO440 instrument equipped with an InLens detector (acceleration voltage, 2.0 kV).

(12) (a) Furubayashi, Y.; Hitosugi, T.; Yamamoto, Y.; Inaba, K.; Kinoda, G.; Hirose, Y.; Shimada, T.; Hasegawa, T. *Appl. Phys. Lett*. **2005**, *86*, 252101. (b) Lu, X. J.; Mou, X. L.; Wu, J. J.; Zhang, D. W.; Zhang, L. L.; Huang, F. Q.; Xu, F. F.; Huang, S. M. I. *Adv. Funct. Mater*. **2010**, *20*, 509.
(13) Cui, H.; Dwight, K.; Soled, S.; Wold, A. *J. Solid State Chem*. **1995**, *115*, 187.
(14) Okazaki, S.; Okuyama, T. *Bull. Chem. Soc. Jpn*. **1983**, *56*, 2159.
(15) Zakrzewska, K.; Radecka, M.; Rekas, M. *Thin Solid Films* **1997**, *310*, 161.
(16) (a) Qiao, H.; Xiao, L. F.; Zhang, L. Z. *Electrochem. Commun*. **2008**, *10*, 616. (b) Guo, Y. G.; Hu, Y. S.; Maier, J. *Chem. Commun*. **2006**, 2783. (c) Guo, Y. G.; Hu, Y. S.; Sigle, W.; Maier, J. *Adv. Mater*. **2007**, *19*, 2087. (d) Kubiak, P.; Geserick, J.; Hüsing, N.; Wohlfahrt-Mehrens, M. *J. Power Sources* **2008**, *175*, 510.
(17) (a) Bavykin, D. V.; Friedrich, J. M.; Walsh, F. C. *Adv. Mater*. **2006**, *18*, 2807. (b) Cheng, F.; Chena, J. *J. Mater. Res*. **2006**, *21*, 2744.
(18) Antonietti, M.; Ozin, G. A. *Chem.—Eur. J*. **2004**, *10*, 28.
(19) Thomas, A.; Schlaad, H.; Smarsly, B.; Antonietti, M. *Langmuir* **2003**, *19*, 4455.
(20) Djerdj, I.; Arčon, D.; Jagličić, Z.; Niederberger, M. *J. Phys. Chem. C* **2007**, *111*, 3614.

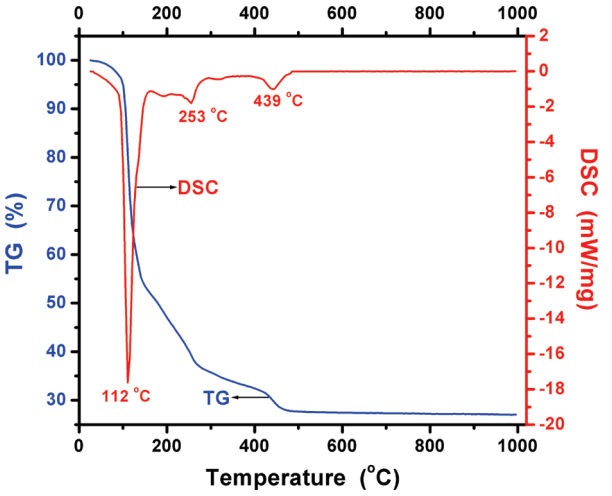

Figure 1. DSC and TGA curves of as-synthesized NTO sample.

The samples for SEM were prepared by dispersing the final powders in the conductive glue; this dispersing was then sprayed with gold. N_2 adsorption−desorption isotherms at 77 K were recorded on a Micromeritics ASAP 2010 automated sorption analyzer. The samples were outgassed 20 h at 150 °C before the analysis.

Conductivity Measurement. Conductivity measurement was performed on NTO pellets (13 mm in diameter) prepared from about 200 mg of powder in an evacuated press under a pressure of 15 tons. The cold-pressed pellet was directly used for the measurements without any additional thermal treatment. The pellet was contacted between the gold-plated cylindrical electrodes acting both as voltage and current leads. Resistance across the pellet was measured by a digital multimeter (Keithley Instruments, model 2000) in a four-probe mode for eliminating the undesired resistance of the measuring circuit. The specific conductivity S was calculated from the measured resistance R as $S = H/RA$, where A is the electrode area and H is the pellet thickness.

Electrochemical Characterization. Electrochemical experiments were performed using Swagelok-type cells. The working electrodes were prepared by mixing the TNHCs, carbon black, and poly(vinyl difluoride) (PVDF) at a weight ratio of 70:15:15 and were pasted on pure Cu foil (99.6%, Goodfellow). Glass fiber (GF/D) from Whatman was used as a separator. The electrolyte consists of a solution of 1 M LiPF6 in ethylene carbonate (EC)/dimethyl carbonate (DMC) (1:1, in volume) obtained from UbeIndustries Ltd. Pure lithium foil (Aldrich) was used as a counter electrode. The discharge and charge measurements were carried on an Arbin MSTAT system. The cells were assembled in an argon-filled glovebox. Cyclic voltamogram experiment was performed on a Voltalab 80 electrochemical workstation at a scan rate of 0.2 mV s^{-1}.

Results and Discussion

The TGA and DSC measurements were carried out in a flowing air atmosphere to analyze the decomposition process of the as-synthesized NTO. Thermogravimetric analysis (TGA) of the as-synthesized intermediate (after drying in air at room temperature for 24 h) under air shows a ~72 wt % total weight loss in three apparent steps on heating to 470 °C (Figure 1). The first occurs over the temperature range from room temperature to ~112 °C,

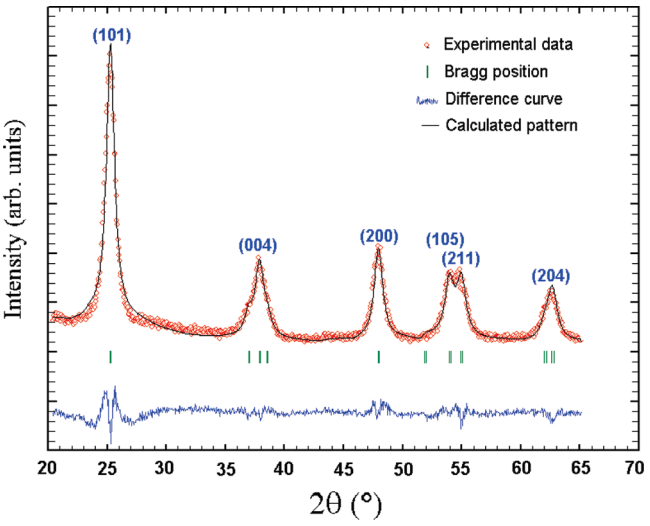

Figure 2. X-ray diffraction analysis of the mesoporous NTO with 6.5% Nb doping. The experimental data is shown in red, the calculated patterns in black, and the difference curves in blue. The short vertical bars in green represent the positions of the Bragg reflections.

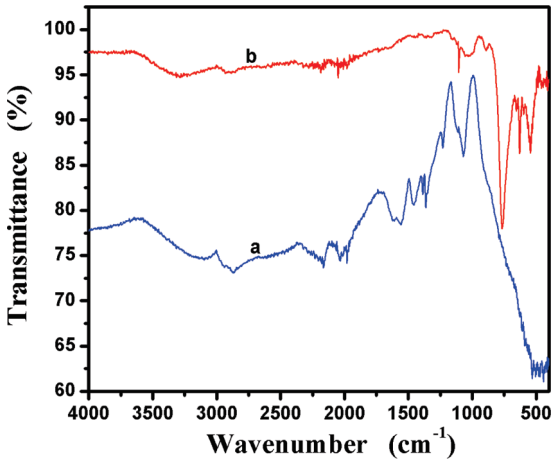

Figure 3. FTIR spectra of NTO samples: (a) as-prepared and (b) after calcination at 470 °C for 2 h.

the second over the temperature range from 112 °C to ~253 °C, the third is at 253−470 °C. Presumably, the first step is attributable to the release of chemically bound residual solvent, adsorbed water, and surface hydroxylated species. This process corresponds to about ~45% total weight loss, while the second one to desorption and decomposition of the polymer KLE.[21] In the range of 253−470 °C, polymer KLE completely decomposes and crystalline TiO_2 is formed. As the weighted-in polymer content is only 37.2 wt %, ~35 wt % mass loss has to be attributed to the removal of organic solvents, mainly EtOH and THF, bound within the amorphous NTO-intermediate. Little further weight loss in the TGA curve was observed at a temperature above 470 °C, indicating the completion of any reaction involving a weight change. Because of the much lower heating rate in the synthesis (TGA measurements were performed with 10 °C/min, in contrast to only 1 and 2 °C/min heating in the calcination

(21) Fan, J.; Wang, T.; Yu, C. Z.; Tu, B.; Jiang, Z. Y.; Zhao, D. Y. *Adv. Mater.* **2004**, *16*, 1432.

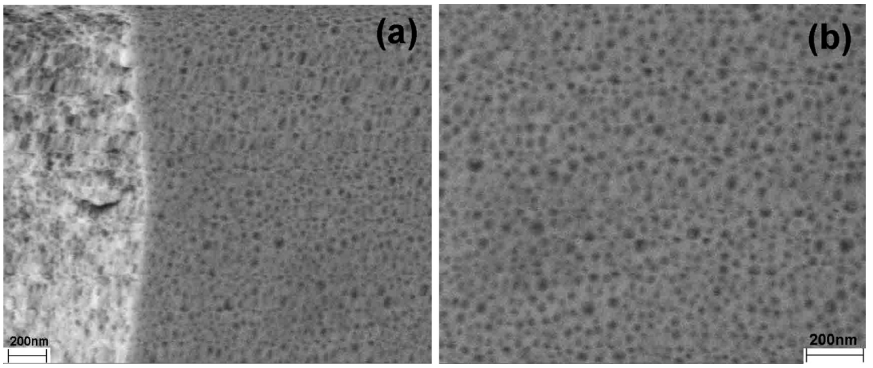

Figure 4. SEM images of (a) cross section and (b) overview of the surface of the mesoporous NTO.

program which in addition contained 2 h holding steps at 300 and 470 °C, respectively), it is therefore safe to say that the organics have been removed in the calcination step.

The experimental XRD pattern of NTO powders, together with the calculated pattern obtained from the Rietveld refinement accompanied by the difference profile are shown in Figure 2. The experimental XRD pattern shows well-developed diffraction lines of anatase TiO_2 (ICDD PDF No. 89-4921), space group $I4_1/amd$ (141). No other crystalline byproduct such as NbO_2 or Nb_2O_5 were found in the pattern, indicating that the as-synthesized sample had anatase structure. For all investigated materials, the refined values of lattice parameters and unit-cell volume of Nb-doped TiO_2 anatase are very close to ICDD values (a = 3.7845 Å, c = 9.5143 Å, V = 136.27 Å^3). The ionic radius of Nb^{5+} (0.64 Å) in octahedral environment is very similar to Ti^{4+} ionic radius (0.605 Å) in the same coordination. It implies that the niobium doping most probably occurs by substituting the titanium atom in the crystal structure, otherwise the lattice parameters of anatase would deviate more from the undisturbed ICDD values The average crystallite size (D) of the NTO was calculated by applying the Scherrer equation to the (101) diffraction peak (2θ = 25.2°). The average crystallite size is 7.1 nm. The structure of the NTO was refined by the Rietveld method applied on the XRD powder pattern, and the values of unit cell parameters, fractional atomic coordinates, and the average crystallite size are listed in Table S1 of the Supporting Information. The broadening of the peaks points to a small crystallite size, which is confirmed by the Rietveld refinement that gives a volume-weighted average crystallite size of 7.3 nm. The result is in a good agreement with the average crystallite size calculated by using the Scherrer equation. The characterizations of the samples doped with various Nb contents pointed out that the only crystalline phase is TiO_2 anatase phase and Nb atoms enter substitutionally to Ti atoms in the bulk titania structure; finally the Nb concentration can be modulated up to ~20 at % without segregation of Nb oxides (Figure S1 of the Supporting Information).

The calcined and uncalcined samples were also studied by FTIR, respectively. The FTIR spectra were analyzed in the 400 and 4000 cm^{-1} range, as shown in Figure 3. Their results demonstrate that KLE has been completely decomposed due to the disappearance of the characteristic absorption peaks of carbonyl. From XRD data, the existence of any crystal compounds containing niobium cannot be found. So, FTIR was also used to characterize the framework structure to find out in which form niobium exists in the sample. From the FTIR spectra, the absorptions observed around 556 and 460 cm^{-1} are related to vibrations of the TiO_2 lattice.[22] A peak at 768 cm^{-1} is seen for the Nb-doped TiO_2 samples which can be assigned to Nb−O−Ti vibrations. The peak shifting (at 545 cm^{-1}) in the vibrations of the TiO_2 lattice seen around 556 cm^{-1} ascertains the substitution of the Ti sites with Nb in the TiO_2 lattice.[23] In the IR spectra of our samples, the vibration corresponding to pure Nb_2O_5 (two characteristic vibration peaks, at 642 and 1650 cm^{-1}, as well as a shoulder at 941 cm^{-1}), NbO (970 cm^{-1}), and NbO_2 (876 cm^{-1}) did not appear, indicating that niobium could be introduced into the titania framework in the form of Nb−O−Ti bonds.

As can be seen from Figure 4, the NTO powders clearly show the mesoporous character with the pore size of 10−20 nm. Figure 4a presents the internal structure of NTO and confirms the highly porous structure. In Figure 4b, one can see that the surface of NTO is very flat and with many disordered pores open to the surface. These figures also give us a very straightforward feeling that the material has high surface area. By using the ultrahigh resolution SEM, we did not observe any contrasts on the SEM images for the NTO sample. This may suggest that there is no segregation in the Nb_2O_5 state between TiO_2 crystallites. Hence, the sample is bulk doped.

The mesoporosity was further investigated by transmission electron microscopy (TEM), and the images are presented in Figure 5. From Figure 5a, it can be seen that it is highly porous, but all the pores are randomly organized. The high crystallinity of the powder leads to well-pronounced Debye−Scherrer diffraction rings in the SAED pattern (Figure 5b) that can be assigned to the reflections (101), (004), (200), and (105) planes of anatase TiO_2, respectively. These indexed patterns are in good

(22) Nakamura, R.; Imanishi, A.; Murakoshi, K.; Nakato, Y. *J. Am. Chem. Soc.* **2003**, *125*, 7443.
(23) Teixeira, Z.; Alves, O. L.; Mazali, I. O. *J. Am. Ceram. Soc.* **2007**, *90*, 256.

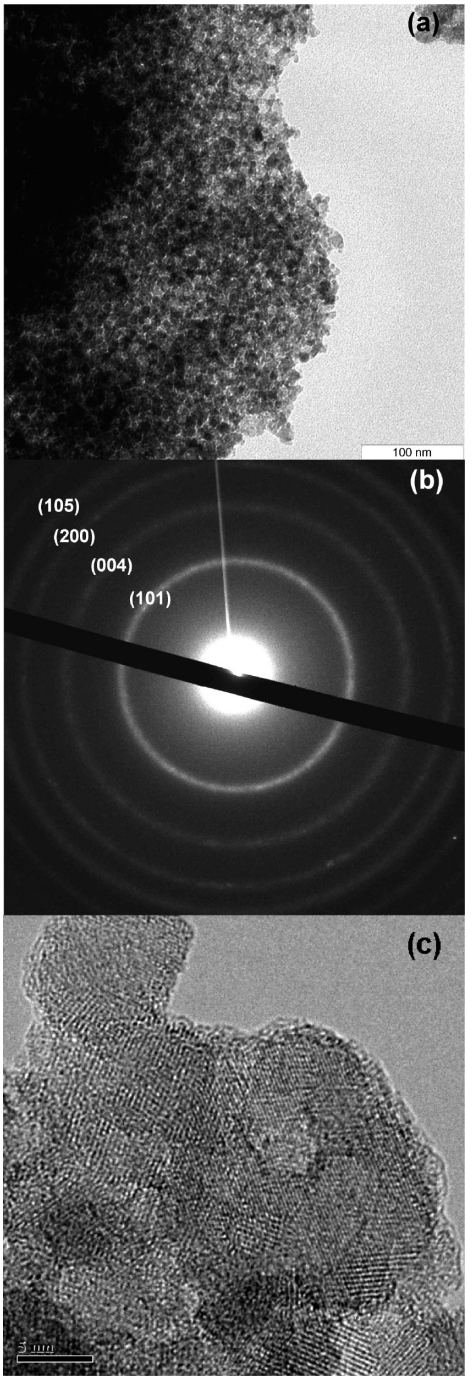

Figure 5. (a) TEM image of the mesoporous NTO, (b) selected area electron diffraction, and (c) HRTEM image of the mesoporous NTO.

accordance with the XRD reflections described above. There are no additional rings in the SAED pattern stemming from any crystalline impurities. The high crystallinity of NTO nanoparticles as well as the pore morphology was further characterized by the corresponding HRTEM in Figure 5c. It confirms that the pore walls are mostly crystallized and the nanoparticles building up the wall of the pores are all highly crystalline. Moreover, the nanocrystals attach to each other randomly without any preferred orientation, which coincides with the conclusion drawn on the XRD pattern. The pore shape in this image looks quite irregular. However, the regularity of

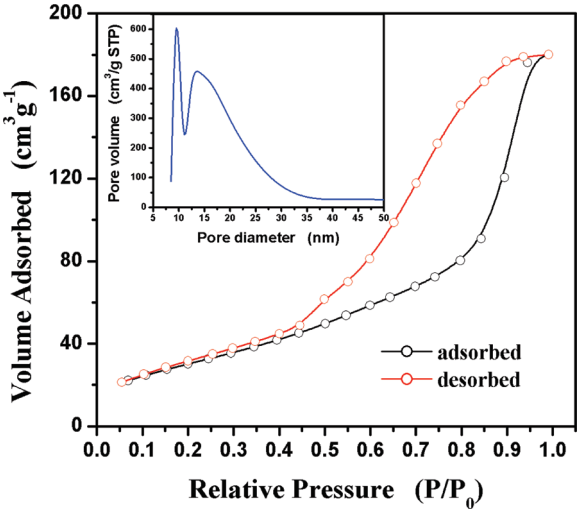

Figure 6. Nitrogen adsorption/desorption isotherms with pore size distribution and the inset for the mesoporous NTO.

the pore shape and the porous structure are not very important for the surface area and the catalytic properties based on the previous studies.[18,24]

BET nitrogen adsorption−desorption isotherms and pore size distribution measurements were performed. The adsorption−desorption isotherm with the evident hysteresis loops can be found in Figure 6. The isotherm is of type IV characterized by a broad hysteresis loop, which proves the presence of mesopores within the NTO powders. Its specific surface area from BET measurement is approximately 128 m^2/g and the total pore volume amounted to 0.211 cm^3/g. The steep adsorption and desorption branches indicate that NTO powders possess a narrow pore size distribution. The Figure 6 inset shows that there are two maximum pore size distributions for NTO. It is centered at 9.7 and 14.7 nm.

The composition of the NTO was further analyzed by XPS. Apart from the C1s peak positioned at 286.0 eV, which originated from spurious amounts of surface carbon of the decompsed KLE polymer template adsorbed onto the inorganic framework of NTO, the XPS survey spectrum (Figure S2a,b of the Supporting Information) confirmed the high chemical purity of the NTO nanoparticles, consisting solely of Ti, Nb, and O. However, the undoped mesoporous TiO_2 only showed the composition of Ti and O (Figure S2c,d of the Supporting Information). The high-resolution XPS spectrum of Nb-doped TiO_2 is reported in Figure 7. The position of the Ti $2p_{3/2}$ peak at 458.75 eV with a better symmetry is close to the value reported for Ti^{4+} (458.7 eV).[25] The distance between these two peaks was 5.6 eV, being in good agreement with the energy splitting reported for TiO_2. The values correspond to the 2p binding energy of Ti(IV) ions (indexed Standard ESCA Spectra of the Elements and Line Energy Information, Φ Co.). As expected in TiO_2, the oxidation state of titanium is 4+, and it appears that the TiO_2 phase has not

(24) Rolison, D. R. *Science* **2003**, *299*, 1698.
(25) Briggs, D.; Rivière, J. C. *Practical Surface Analysis by Auger and X-ray Photoelectron Spectroscopy*; Briggs, D., Seah, M. P., Eds.; John Wiley & Sons: London, 1983; pp 87−139.

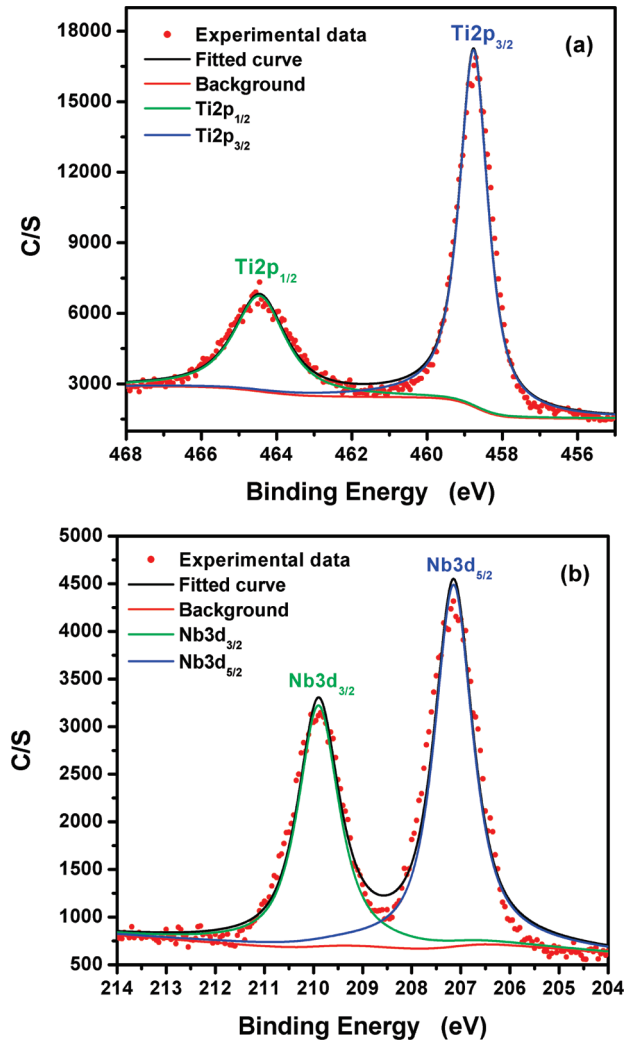

Figure 7. The high-resolution XPS spectra of superposed Ti2p (a) and Nb3d (b) for the mesoporous NTO.

been changed by the Nb doping. Concerning the Nb 3d spectra for NTO, two peaks are observed whose binding energies are 207.1 eV for the Nb $3d_{5/2}$ peak and 209.9 eV for the Nb $3d_{3/2}$ peak, respectively, with a spin-orbit splitting of 2.8 eV. In Figure 7a, the Nb_2O_5 $3d_{5/2}$ symmetry peak can be modeled by a single Gaussian peak centered at 207.1 eV. The binding energy for Nb $3d_{5/2}$ for $Nb(V)_2O_5$ is about 207.4 ± 0.4 eV.[26] The result suggests that the oxidation state of Nb in the Nb-TiO_2 is mainly 5+. The analysis of the O 1s XPS peak (Figure S3a of the Supporting Information) provides conclusive evidence of Nb−O−Nb contacts within the anatase structure. Two different contributions are observed among the samples of TiO_2 and Nb-doped TiO_2 prepared in this study (Figure S3 of the Supporting Information); the first is associated to oxygen lattice ions of the anatase network (~530.0−530.5 eV) and the second with surface hydroxyls at titania surfaces (~530.9−531.5 eV). The results indicate that niobium atoms replace titanium atoms and assume the same oxidation state of 4+ as titanium atoms. Thus, they can increase the electrical conductivity as donors impurities as it shown by the following chemical reaction:

$$Nb_2O_5 \leftrightarrow 2Nbi^{\bullet}Ti + 4O_o + 2e' + \frac{1}{2}O_2$$

The electrical conductivity of NTO was measured by pressing the material into pellets with no further heat-treatments. The electrical conductivity measured on pressed and palletized mesoporous NTO was approximately 2.86×10^{-6} S cm^{-1}. In comparison to the result of the undoped TiO_2 with mesoporosity (conductivity 2.38×10^{-8} S cm^{-1}), the conductivity of mesoporoous NTO with 6.5% Nb content is more than 2 orders of magnitude higher.

To evaluate the potential applicability in high-power Li batteries, we investigated fundamental electrochemical properties of the as-prepared NTO with respect to Li insertion/extraction. The insertion and extraction of lithium to and from the anatase lattice proceeds according to the eq 1. The theoretical capacity, 336 mA h g^{-1}, of TiO_2 will be obtained when x equals 1. The insertion coefficient, x, in anatase is usually close to 0.5 at slower charging/discharging rate.[27] The first cycle charge−discharge curve at a constant current of ~$C/6$ with a cutoff voltage window of 1−3.1 V is shown in Figure 8a. As can be seen from Figure 8a, there is a distinct charge and discharge voltage plateau related to the redox peaks in the CV, indicating the typical electrochemical characteristics of anatase TiO_2. There is a distinct potential plateau at 1.69 and 1.96 V for discharging (Li insertion) and charging (Li extraction), respectively. It is similar to the potential plateaus observed in other literature.[28] The first cycle discharge capacity for the NTO is 238 mA h g^{-1}, and the corresponding charging capacity is 167 mA h g^{-1}. Figure 8b shows the plot of discharge/charge capacity vs cycle number of the mesoporous NTO sample at a current rate of $C/6$. The initial discharge capacity is about 238 mA h g^{-1}, accompanied with a capacity fluctuation between 151 and 162 mA h g^{-1} after 60 cycles and then gradually leveling off at 160 mA h g^{-1}, which indicates a good cycling performance. The discharge/charge capacity is 160 mA h g^{-1} with a Coulombic efficiency of 99.8% with an excellent cycling stability even in the 100th cycles at a rate of $C/6$. The results demonstrate the excellent cycling stability of the mesoporous NTO. As can be seen, for the NTO with mesoporosity, there has been a slower fading and a better electrochemical performance than of the undoped TiO_2 with mesoporosity (Figure S4 of the Supporting Information) and the NTO nanoparticles with 6.5% molar ratio Nb (Figure S5 of the Supporting Information). It is very interesting to note that TiO_2 with the doping 6.5% possess better capacity retention than other samples with the different doping levels even if they have similar mesoporosity and crystal sizes (Table S1 of the Supporting Information). High-rate cycling behavior

(26) Mattsson, A.; Leideborg, M.; Larsson, K.; Westin, G.; Osterlund, L. *J. Phys. Chem. B* **2006**, *110*, 1210.

(27) Sun, X. D.; Ma, C. L.; Wang, Y. D.; Li, H. D. *Nanotechnology* **2004**, *15*, 1535.

(28) (a) Stashans, A.; Lunell, S.; Bergstrom, R.; Hagfeldt, A.; Lindquist, S. E. *Phys. Rev. B* **1996**, *53*, 159. (b) Xu, J. W.; Jia, C. H.; Cao, B.; Zhang, W. F. *Electrochim. Acta* **2007**, *52*, 8044.

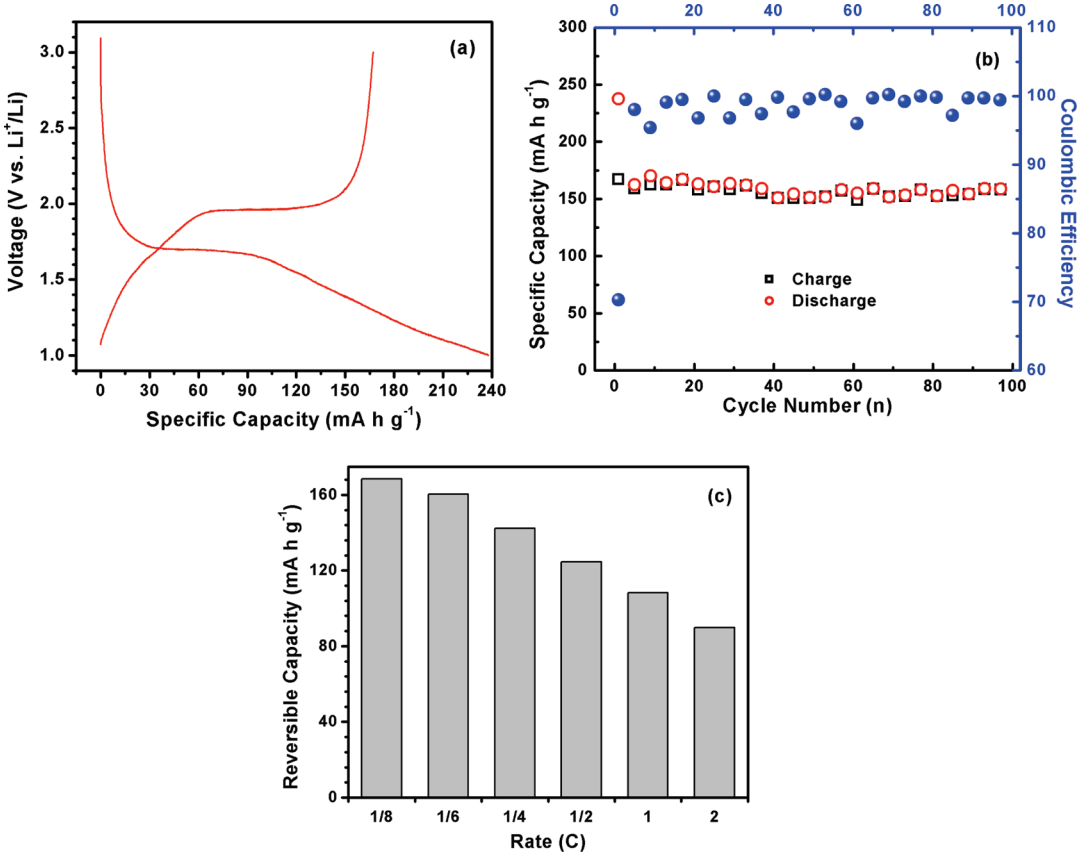

Figure 8. The galvanostatic voltage profiles between 1 and 3.1 V for the first cycle (a), the discharge/charge capacity profile and Coulombic efficiency between 1 and 3.1 V voltage window and *C*/6 up to the hundredth cycle (b), and cycling and rate performance (c) of the mesoporous NTO electrode cycled at *C*/8, *C*/6, *C*/4, *C*/2, 1*C*, and 2*C*.

is one of the most important electrochemical characteristics of lithium-ion batteries required for power storage application. Different scan rates were applied to study the influence of the high surface area and the pore transport system on the electrochemical properties of NTO here. As it might have been expected from the structural characterization, our mesoporous NTO showed good rate capabilities. The corresponding results are shown in Figure 8c. A reversible capacity of around 168.4 mA h g^{-1} was obtained at a rate of *C*/8 after 10 cycles; this value decreased to 160.3 mA h g^{-1} at *C*/6, 142.4 mA h g^{-1} at 0.25*C*, 124.6 mA h g^{-1} at 0.5*C*, 108.2 mA h g^{-1} at 1.0*C*, and finally, 89.8 mA h g^{-1} at 2.0*C*. The mesoporous NTO electrode not only shows higher rate capability than the anatase TiO_2 electrode but also possesses desirable cycling performance.

The good transport of Li-ion and/or electron in electrodes can improve the charge/discharge rate performance of Li-ion batteries. To increase electron transport in the TiO_2 electrode materials, a variety of approaches have been developed, such as conductive coating[29] and uses of conductive additives.[16c] TiO_2 nanotubes were decorated with Ag prepared by the traditional silver mirror reaction to improve the electronic conductivity and the electrochemical performance.[29] The mesoporous TiO_2 introduced a suitable electronic conducting nanosized 3D network RuO_2, which provides negligible diffusion times, enhanced local conductivities, and possibly faster phase transfer reactions, that shows the outstanding rate performance.[16c] For the mesoporous NTO electrode material, such a good performance may be attributed to the high electronic conductivity and the mesoporous structures, thus enabling an improved dynamics for both electronic and Li^+ transport as well as a high electrode−electrolyte contact area. With comparison with the mesoporous Nb-doped TiO_2 electrode using carbon black, the electrochemical performance does not have the distinct changes for the electrode without using conducting additives (Figure S6b of the Supporting Information). However, for the mesoporous TiO_2 electrode without using conducting additives, the battery performance distinctly reduces (Figure S6a of the Supporting Information). One can find the significance of the effect of Nb doping on the electrode performance. In recent years, the pseudocapacitive effect has been observed in high surface area mesoporous materials. Our samples are just constructed with mesopores, so it is likely that the mesoporous structures facilitate the pseudocapacitive behavior.

In summary, niobium-doped TiO_2 with mesoporosity and high surface area was successfully prepared by using a novel amphiphilic diblock copolymer KLE22 as the template in an alcohol system. The TEM, XRD, FTIR, and XPS results showed that the Nb was indeed incorporated into the TiO_2 crystal structure (anatase TiO_2). The total pore volume, surface area, two maximum pore

(29) He, B. L.; Dong, B.; Li, H. L. *Electrochem. Commun.* **2007**, *9*, 425.

size distributions of mesoporous NTO were 0.211 cm^3/g, 128 $m^2\ g^{-1}$, 9.7 nm, and 14.7 nm, respectively. This mesoporous anatase showed good electrochemical performance when it was used as a cathode for a lithium battery. A highly stable capacity of 160 mA h g^{-1} was found after 100 cycles. Its excellent cycling behavior makes it a promising cathode material for advanced electrochemical devices for lithium-ion batteries.

Acknowledgment. The authors thank Xinglong Wu and Professor Yuguo Guo (Beijing National Laboratory for Molecular Sciences Institute of Chemistry, Chinese Academy of Sciences (CAS), Beijing China) and Tingting Ma (Kunming University of Science and Technology, China) for the electrochemical characterization. One of the authors (Y. D. Wang) acknowledges the financial support from the Alexander Humboldt Society in the form of a fellowship.

Supporting Information Available: Structural data and refinement parameters for NTO mesoporous structures calculated by Rietveld refinement of the experimental XRD powder pattern, XPS survey and O1s signal spectra of NTO mesoporous structures, and conductivity data and electrochemical characterization of Nb-doped titania mesoporous structures with different Nb contents (PDF). This material is available free of charge via the Internet at http://pubs.acs.org.